Differing Conformational Pathways Before and After Chemistry for Insertion of dATP versus dCTP Opposite 8-OxoG in DNA Polymerase β

Yanli Wang,* Sujatha Reddy,* William A. Beard,[†] Samuel H. Wilson,[†] and Tamar Schlick*

*Department of Chemistry and Courant Institute of Mathematical Sciences, New York University, New York, New York; and [†]Laboratory of Structural Biology, National Institute of Environmental Health Sciences, National Institutes of Health, Research Triangle Park, North Carolina

ABSTRACT   To elucidate how human DNA polymerase β (pol β) discriminates dATP from dCTP when processing 8-oxoguanine (8-oxoG), we analyze a series of dynamics simulations before and after the chemical step with dATP and dCTP opposite an 8-oxoG template started from partially open complexes of pol β. Analyses reveal that the thumb closing of pol β before chemistry is hampered when the incorrect nucleotide dATP is bound opposite 8-oxoG; the unfavorable interaction between active-site residue Tyr[271] and dATP that causes an *anti* to *syn* change in the 8-oxoG (*syn*):dATP complex explains this slow motion, in contrast to the 8-oxoG (*anti*):dCTP system. Such differences in conformational pathways before chemistry for mismatched versus matched complexes help explain the preference for correct insertion across 8-oxoG by pol β. Together with reference studies with a nonlesioned G template, we propose that 8-oxoG leads to lower efficiency in pol β's incorporation of dCTP compared with G by affecting the requisite active-site geometry for the chemical reaction before chemistry. Furthermore, because the active site is far from ready for the chemical reaction after partial closing or even full thumb closing, we suggest that pol β is tightly controlled not only by the chemical step but also by a closely related requirement for subtle active-site rearrangements after thumb movement but before chemistry.

INTRODUCTION

DNA base and sugar lesions caused by cellular reactive oxygen species contribute to mutagenesis and carcinogenesis (1). One of the most prevalent lesions in the genome is 7, 8-dihydro-8-oxoguanine (8-oxoG) (2) (Fig. 1 *b*), in which C8 is oxidized to a carbonyl group and N7 is transformed to an –NH– group. The 8-oxoG nucleoside can adopt two gly-cosidic conformations: the *anti* conformation when paired with a complementary **C** (Fig. 1 *c*), and the *syn* conformation when paired with **A** to form a Hoogsteen basepair (Fig. 1 *d*); the latter avoids a clash between the deoxyribose backbone and the 8-oxo group. When it is not repaired, the mismatched 8-oxoG:A basepair can introduce **G:C** to **T:A** transversion mutations (i.e., the mispairing of 8-oxoG with **A** will result in thymine in the next replication cycle). Such mutations contribute significantly to somatic mutations associated with spontaneous cell transformations (3–6).

High- and low-fidelity DNA polymerases, such as human DNA polymerase β and *Sulfolobus solfataricus* P2 DNA polymerase IV (Dpo4), often encounter 8-oxoG (7–11) and can bypass it in the replication or repair process. Steady-state kinetic data suggest that pol β prefers dCTP over dATP incorporation by twofold and that dCTP insertion is only threefold less efficient opposite 8-oxoG than opposite a normal d**G** (12).

A partial explanation to the accommodation of 8-oxoG: dCTP comes from the ternary crystal structure of the pol β/substrate complex with 8-oxoG (13): the structure shows that the matched 8-oxoG (*anti*):dCTP basepair is easily tolerated by pol β due to a 184° flip of the template backbone (O3′-P-O5′-C5′), thereby avoiding the clash between O8 and O5′ and O1P of 8-oxoG. The mismatched 8-oxoG (*syn*):dATP basepair, in contrast, is not as stable as the matched pair in pol β. Crystallography has not captured the *syn* conformation of 8-oxoG pairing with dATP in pol β but rather captured *anti* 8-oxoG stacking with dAMP (12).

Besides the crystal structures of pol β 8-oxoG complexes, other DNA polymerases across different families with 8-oxoG at the template position have also been resolved crystallographically. These include RB69 from the B-family (10), T7 DNA polymerase (14,15) and *Bacillus* fragment (BF) from the A-family (11), and Dpo4 from the Y-family (16). However, none of these wild-type enzyme complexes captured *syn* 8-oxoG pairing with dATP at the active site. Recently, only by mutating Lys[536] to Ala has the ternary form of T7 DNA polymerase resolved the 8-oxoG (*syn*):dATP basepair (15).

Kinetic data for pol β, RB69, Dpo4, wild-type T7, Lys[536]Ala T7, and BF (10–12,15,16) indicate preference ratios of dCTP over dATP incorporation opposite 8-oxoG to be 2:1, 20:1, ~70:1, 2:1, 1:20, and 1:9, respectively. We thus can infer that the incorporation of 8-oxoG (*syn*):dATP mismatch is energetically less favorable in pol β, wild-type T7, RB69, BF, and Dpo4, but more favorable in Lys[536]Ala T7, than the corresponding 8-oxoG (*anti*):dCTP basepair.

Although the nascent basepair 8-oxoG:dAMP is distorted in the pol β/DNA crystal structure, a modeling of dATP pairing with *syn* 8-oxoG in the closed pol β revealed no serious steric clashes at the active site (17). Since pol
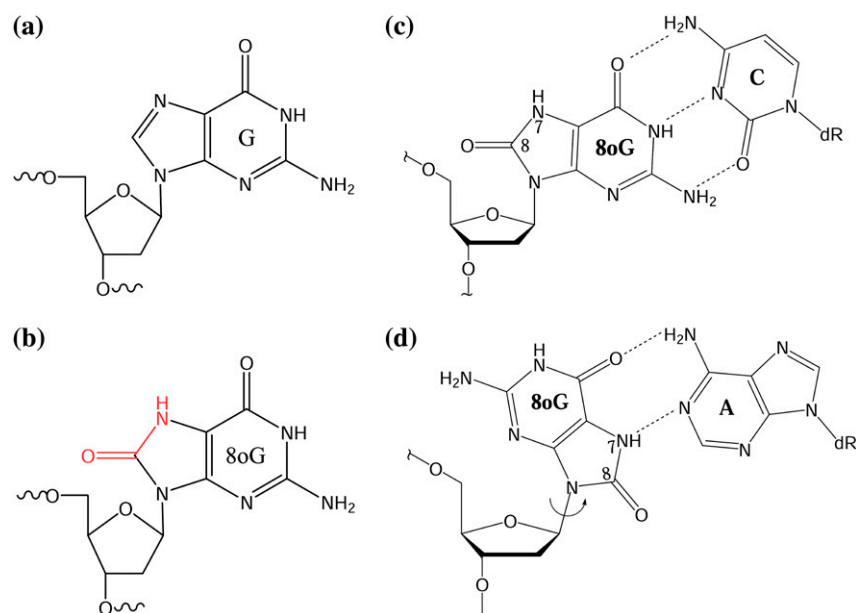
FIGURE 1 The molecular formulas of guanine (*a*) and 8-oxo**G** (*b*) and the two possible 8-oxo**G** pairing forms: (*c*) *anti* Watson-Crick pairing, with **C**; and (*d*) *syn* Hoogsteen pairing, with **A**.

β maintains fidelity in DNA replication through an induced-fit mechanism—the thumb subdomain of pol β closes when the correct nucleotide complementary to the template residue binds (18–22) and opens after the chemical reaction to release the reaction products and translocate DNA—the induced-fit cycle may also contribute to differentiating d**ATP** and d**CTP** insertions opposite 8-oxo**G** and d**G** (12). Specifically, d**ATP** is less efficiently inserted opposite 8-oxo**G** than d**CTP** in pol β, though d**ATP** insertion is $\sim 10^5$ more efficient compared with it opposite d**G**. Furthermore, computational studies of pol β (22–28) have shown that conformational pathways of pol β before and after the chemical reaction play a vital role in determining its fidelity. With the ultimate goal of understanding the fidelity mechanism of pol β in processing 8-oxo**G**, we investigate here the dynamic process of pol β's conformational pathways before and after the chemical reaction by performing a series of six dynamics simulations starting from intermediate (partially open) structures where the incoming nucleotides d**CTP** and d**ATP** pair with 8-oxo**G** in *anti* or *syn* orientations. Although insertion rates of d**ATP** and d**CTP** opposite 8-oxo**G** in pol β differ slightly, atomic-level simulations can help unravel systematic differences in their conformational pathways to explain biological observations. In fact, our transition path sampling simulations further dissected the conformational and energetics pathways of correct and incorrect nucleotide insertions opposite 8-oxo**G** in pol β (29). The resolved free energy barriers in that work along with the results here suggest that the different transition states and sequences of conformational events during thumb closing for the two systems could be correlated to different stabilities of the respective closed states and associated insertion efficiencies.

In free duplex DNA, 8-oxo**G** assumes an *anti* conformation when pairing with d**C** and a *syn* conformation when situated opposite d**A** (30). Besides these two pairing conformations, we also simulated intermediate structures of a pol β/DNA complex with 8-oxo**G** (*anti*):d**ATP** to exhaust all possibilities.

COMPUTATIONAL METHODOLOGY

System preparation

The intermediate structures of pol β/DNA complexes were constructed by averaging the PDB entries 1BPX and 1BPY for simulations before chemistry and averaging 1BPY and 1BPZ for simulations after chemistry as in previous works (22,23). We started from these intermediate forms to accelerate any possible motions involved (23); partially open or intermediate pol β structures have been captured in crystal forms (17). The **G**:**C** nascent basepairs in the intermediate structures were replaced by 8-oxo**G** (*anti*):d**C**(TP), 8-oxo**G** (*syn*):d**A**(TP), and 8-oxo**G** (*anti*):d**A**(TP) basepairs, respectively. The *syn* 8-oxo**G** was obtained by rotating the N-glycosidic bond (N-C1′) of *anti* 8-oxo**G** by 180° and relaxing the structure. The missing coordinates for protein residues 1–4 in the open gapped binary complex (1BPX) and 1–9 in the ternary closed complex (1BPY) were modeled using Insight II program. All hydrogen atoms were added using CHARMM (31–33). We did not constrain the torsion angle of O3′-P-O5′-C5′ in the simulation for 8-oxo**G** (*anti*):d**CTP** to test whether the steric hindrance between the 8-oxo and O5′ atoms of 8-oxo**G** drives the template backbone to rotate as observed in the ternary crystal structure (13). Indeed, our simulation did show that this backbone dihedral angle rotates by $\sim 180°$ and the O8 $\cdots$ O5′ distance increases from 5.7 to 6.8 Å.

For simulations before chemistry, the nucleotide-binding and catalytic magnesium ions were kept at the active site. For those after chemistry, the chemical reaction was performed manually by connecting 3′-O of the primer terminus and P_α of the incoming nucleotide. The pyrophosphate product and the binding magnesium ions were removed from the active site.

The six pol β/DNA intermediate complexes (three before and three after chemistry) were solvated in face-centered water cubes using Simulaid (34)

and PBCAID (35). The smallest image distance was chosen as 16 Å. Water molecules within 1.8 Å of the heavy atoms of the crystal structure were removed. To neutralize the system and produce an ionic strength of 150 mM, sodium and chloride ions were added by replacing the water oxygens bearing most negative and most positive electrostatic potentials (computed using DELPHI) (36,37), respectively. All ions added were placed at least 8 Å away from the protein or DNA or from each other. The final models contain 41,986 atoms for simulations before chemistry (335 protein residues, 32 nucleotides, 2 Mg^{2+} ions, 21 Cl$^-$ ions, 43 Na$^+$ ions, and 11,830 water molecules), and 41,975 atoms for those after chemistry (335 protein residues, 32 nucleotides, 21 Cl$^-$ ions, 44 Na$^+$ ions, and 11,830 water molecules).

Minimization, equilibration, and dynamics protocol

Periodic boundary conditions and CHARMM27 all-atom force fields for nucleic acids and lipid were used for all energy minimization and MD simulations in CHARMM (32,33).

The force-field parameters for 8-oxoG were adopted from an earlier work (38). The nonbonded interactions were truncated at 14 Å, with van der Waal interactions treated by the switch cutoff method and electrostatic interactions treated by atom-based force-shift method. The performance of different long-range truncation methods have been evaluated by Norberg et al. (39) using a highly charged oligonucleotide in aqueous solution. Results show that the atom-based force-shift method can produce very accurate and stable simulation trajectories and that it is computationally more efficient than the particle-mesh Ewald truncation method.

We minimized and equilibrated the models as follows: the water molecules and hydrogen atoms were minimized using the steepest-decent (SD) algorithm for 10,000 steps with all the other heavy atoms fixed, followed by an adopted-basis Newton-Raphson minimization for 20,000 steps; an equilibration of 10 ps was performed at 300 K by Langevin dynamics to ensure that all the sodium and chloride ions were located on potential energy minima or maxima around the protein/DNA complexes; the entire system was again minimized by SD for 10,000 steps and adopted-basis Newton-Raphson minimization for 20,000 steps with all the protein and DNA heavy atoms fixed; finally, the system was equilibrated with the multiple-timestep Langevin integrator, LN (40–43), for 100 ps with all the atoms released.

For production runs, LN was used with timesteps $\Delta\tau/\Delta t_m/\Delta t$ set at 1/2/150 fs for the fast, medium, and slow force components and a medium-range cutoff of 7 Å and healing and buffer lengths of 4 Å each. The damping constant γ was set to 10 ps^{-1}. The structures before chemistry were simulated for ~18 ns and those after chemistry for 13 ns. SHAKE was applied to all bonds with hydrogen atoms. Coordinates were saved every 3 ps.

RESULTS

Simulations before chemistry suggest nascent-basepair-dependent thumb and side-chain motions in 8-oxoG complexes

Using α-helix N on pol β's thumb subdomain as an index of different enzyme states, we compare the final conformations of simulated complexes to the crystal structures in Fig. 2 (*top*). Results show that the thumb subdomain closes in the 8-oxoG (*anti*):dCTP system, while it is partially open in 8-oxoG (*syn*):dATP and completely open in 8-oxoG (*anti*):dATP. These trends are also evident from the root mean-square deviation (RMSD) plots of α-helix N in Supplementary Material Fig. S1, *a–c*. Note that although the models with different nascent basepairs were built from the same intermediate structures (both before and after chemistry), they
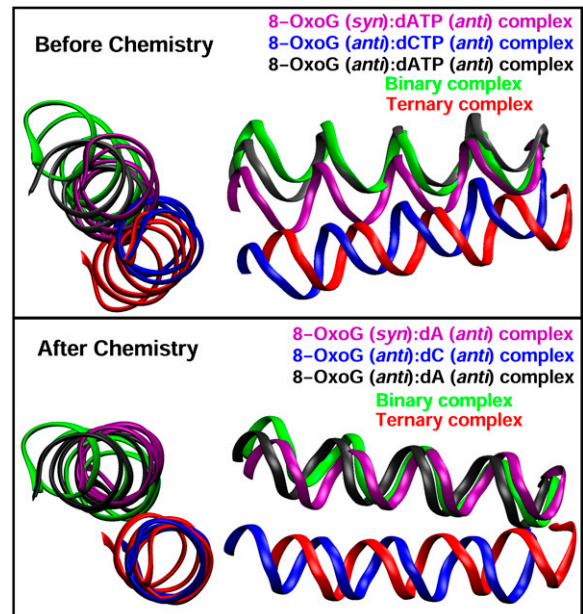

FIGURE 2 Top and side views of α-helices *N* in the simulated pol β complexes before (*top*) and after (*bottom*) the chemical reaction compared with those in the binary and ternary crystallographic structures of pol β (19). Pol β/substrate complexes with the 8-oxoG (*anti*):dC(TP), 8-oxoG (*syn*):dA(TP), and 8-oxoG (*anti*):dA(TP) nascent basepairs are shown in blue, purple, and gray, respectively. Superimposition is performed according to the palm subdomains.

deviate from the initial coordinates during the minimization/equilibration process so that the starting RMSD values on these plots appear different among the three systems.

Crystallographic and computational studies (19,22,23,27) have indicated that a sequence of side-chain rearrangements (Asp^{192} rotation, Phe^{272} flip, and Arg^{258} rotation) occurs at the active site of pol β as it transitions from open to closed states during DNA synthesis. The final conformations of these key residues are displayed in Fig. 3 (*top*). In the 8-oxoG (*anti*):dCTP system, Asp^{192}, Phe^{272}, and Arg^{258} achieve closed states after the simulation, though Phe^{272} oscillates between open and closed states. In the two 8-oxoG:dATP complexes, Asp^{192} is in a closed conformation binding the two magnesium ions, Arg^{258} remains at the intermediate state, and Phe^{272} rotates to the open state (see Supplementary Material Fig. S2 for the time evolutions of dihedral angles).

In sum, thumb and active-site residue motions indicate that pol β closes after the simulation when 8-oxoG (*anti*):dCTP binds, whereas the complex remains partially and completely open when dATP is opposite *syn* and *anti* 8-oxoG, respectively.

Besides these domain and side-chain motions, distortions of the nascent basepairs occur in each 8-oxoG complex. In the complex of *syn* 8-oxoG pairing with dATP, the N-glycosidic angle of the dATP changes from *anti* to *syn* (Fig. 4 *a*, *left*), suggesting unfavorable interactions for dATP incorporation. In contrast, 8-oxoG (*anti*):dATP and 8-oxoG (*anti*):dCTP
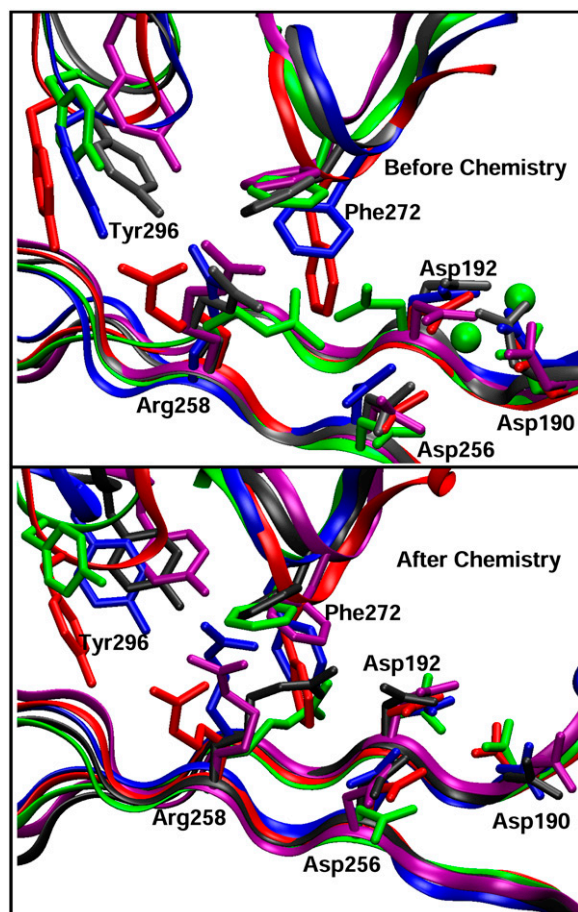
FIGURE 3 Final conformations of the active-site residues in the simulated complexes before (*top*) and after (*bottom*) the chemical reaction compared with those in the binary gapped and ternary crystallographic structures. Superimposition is done according to the palm subdomains. The residue side chains and protein backbones in the complexes with 8-oxo**G** (*anti*):d**C**(TP), 8-oxo**G** (*syn*):d**A**(TP), and 8-oxo**G** (*anti*):d**A**(TP) are colored blue, purple, and gray, respectively. The magnesium ions are shown by green spheres.

are paired and coplanar (Fig. 4, *b* and *c*, *left*), despite being tilted.

More important, even though the thumb and critical residues have attained the closed conformation in the 8-oxo**G** (*anti*):dCTP system, a close examination of the active site reveals that the coordination of the catalytic and nucleotidyl-binding magnesium ions is far from the ideal ''two-metal-ion catalysis'' geometry depicted in Supplementary Material Fig. S3 (44,45). Specifically, the catalytic Mg^{2+} does not coordinate with Asp^{256} but binds 3'-O of the primer terminus, and the $P_\alpha \cdots 3'-O^-$ distance is 6.0 Å, much greater than the ideal value of 3.3 Å (46). In comparison to the geometry of pol β complexed with **G**:dCTP (22), the 8-oxo**G**:dCTP system exhibits large deviations, especially in the binding of the two metal ions, which are positioned farther away from the reaction-competent state. Hence, additional rearrangements are needed to adjust the active-site contents for the nucleotidyl-transfer reaction to occur after
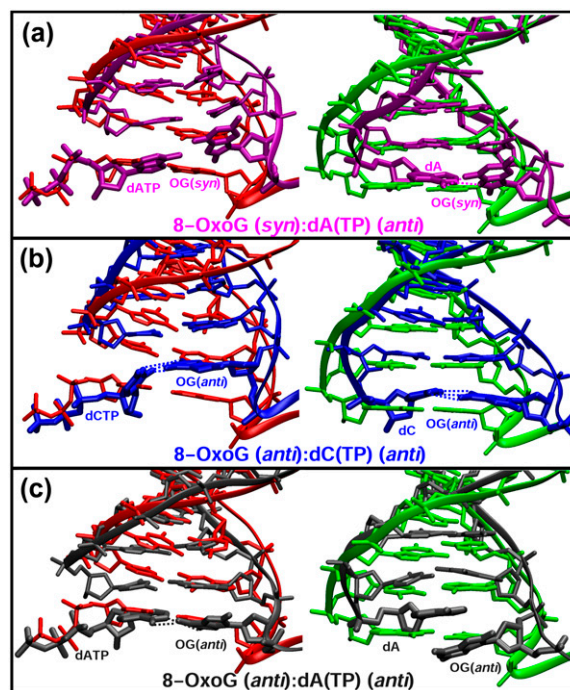
FIGURE 4 The final conformations of the nascent basepairs in the simulated complexes before and after the chemical reaction compared with those of the ternary (*red*) and binary nicked (*green*) crystallographic structures. Color schemes for the three complexes are as labeled.

the thumb closing (see remarks on the pre-chemistry avenue in Discussion).

Tyr[271] might contribute to the preference of Pol β in selecting dCTP versus dATP

Since *syn* 8-oxo**G** prefers to pair with d**A**TP by forming a Hoogsteen basepair in DNA duplexes, it is noteworthy that the nascent bases are distorted and pol β does not close completely in this system before chemistry. To identify the cause, we study the conformations of other active-site residues proximal to the nascent basepair.

We note that Tyr[271] interacts unfavorably with both 8-oxo**G** and d**A**TP bases. As shown in Fig. 5 *a*, unfavorable interactions between Tyr[271] and the 8-oxo**G** (*syn*):d**A**TP basepair in the first 5 ns trigger d**A**TP to rotate from *anti* to *syn* (Fig. 6 *a*) and push 8-oxo**G** toward the DNA major groove (Fig. 6 *b*). After the adenine flip, the interaction energy between 8-oxo**G** and d**A**TP decreases to nearly zero (Supplementary Material Fig. S4 *a*). Furthermore, this base flip also appears to correlate with the thumb subdomain's opening, indicating that distortions caused by Tyr[271] might hinder the thumb's closing for 8-oxo**G** (*syn*):d**A**TP. In comparison, the interactions involving Tyr[271] in the two complexes with *anti* 8-oxo**G** are more favorable (Fig. 6, *b* and *c*).
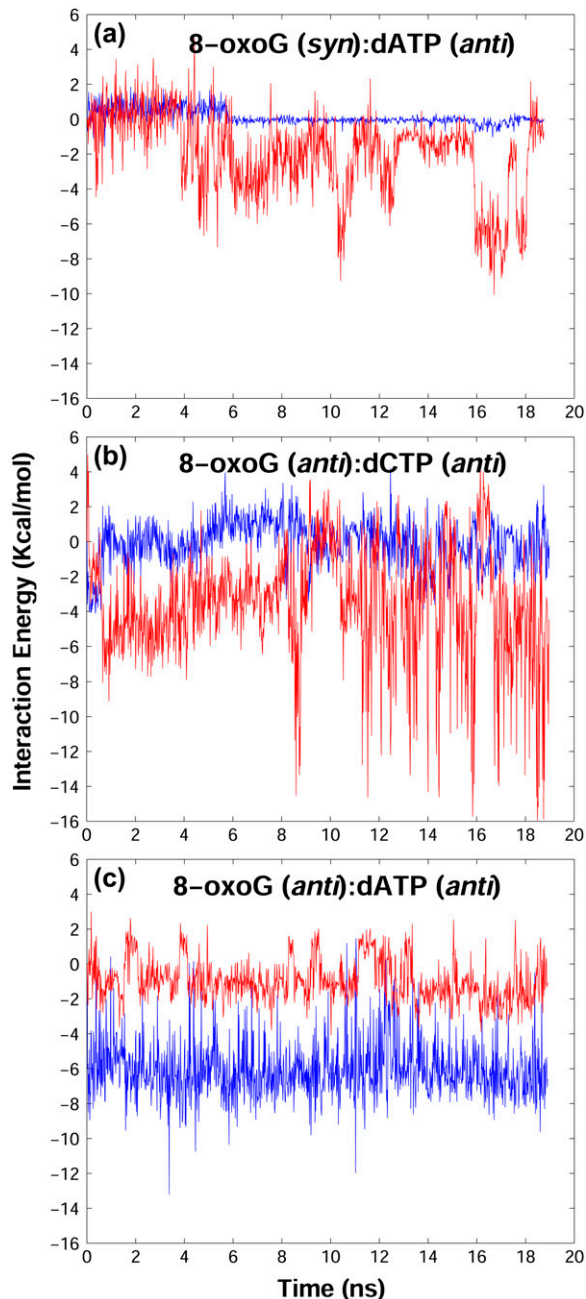
FIGURE 5 Interaction energies between the nascent basepair and Tyr[271] in the simulations before chemistry. Red and blue lines represent the total interaction energies between Tyr[271] and dATP or dCTP, and between Tyr[271] and the template 8-oxoG, respectively.
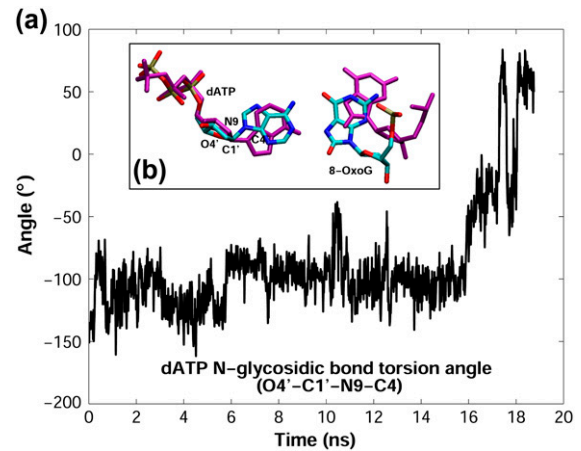

FIGURE 6 (a) Time evolution of the N-glycosidic bond torsion angle of dATP. (b) The initial (atoms in cyan, blue, red, and orange are C, N, O, and P, respectively) and final (purple) conformations of the nascent basepair in the 8-oxoG (syn):dATP pol β complex. Superimposition is performed according to the palm subdomain.

In the crystal structures of closed pol β/DNA complexes with G:dCTP and 8-oxoG:dCTP (13,19), Tyr[271] forms van der Waals contacts with both the sugar ring and base of the incoming nucleotide. The closest atom-to-atom distances are 3.86 Å for sugar ring ⋯ Tyr[271] and 3.23 Å for base ⋯ Tyr[271]. In our simulation for 8-oxoG (syn):dATP, it is the six-membered ring of adenine pointing to Tyr[271] that causes repulsion and triggers dATP's base flip; after the adenine rearrangement, the interactions between dATP and Tyr[271] become favorable.

Thus, our simulations suggest that when pol β encounters 8-oxoG, Tyr[271] might deter the dATP incorporation by destabilizing the nascent basepair and hindering the thumb's closing. This role was confirmed by an MD simulation of the Tyr[271]Ala mutant for the mismatch complex, which reveals that the thumb closes quickly from the intermediate state (data not shown).

Simulations after chemistry show distortions in the 8-oxoG (anti):dA basepair

In the simulations after chemistry, the thumb of pol β opens completely in the two 8-oxoG:dA systems, whereas it closes in 8-oxoG (anti):dC, as shown in Fig. 2 (bottom) (RMSD plots in Supplementary Material Fig. S1, d–f).

Consistent with corresponding thumb motions, active-site residues Asp[192], Arg[258], and Phe[272] change to closed conformation in the 8-oxoG (anti):dC system but flip to their open states in 8-oxoG (anti):dA. In contrast, the 8-oxoG (syn):dA system still has Arg[258] at the intermediate state after Asp[192] and Phe[272] rotate to the open conformation.

Thus, pol β tends to close when anti 8-oxoG pairs with dC but open when syn or anti 8-oxoG pairs with dA. The slow opening of the thumb subdomain for 8-oxoG:dC suggests that it prefers the closed to the open form.

The new basepairs 8-oxoG (syn):dA and 8-oxoG (anti):dC assume Hoogsteen and Watson-Crick conformation after the simulation, respectively (Fig. 4, a and b, right). However, in the 8-oxoG (anti):dA system, dA stacks rather than pairs with the template (Fig. 4 c, right). The base stacking observed here resembles the A:A mismatch found in the

recently solved pol β binary crystal structure (47). The highly distorted 8-oxo**G** (*anti*):d**A** system likely affects the extension rate and induces DNA dissociation and proofreading by an extrinsic exonuclease.

DISCUSSION

Computational and experimental studies on pol β and other polymerases (38,48–50) have suggested that subtle active-site rearrangements may be a key step in the catalytic cycle of these DNA polymerases. In prior works (38,48,51), we have termed these subtle motions in pol β and Dpo4 as the pre-chemistry avenue and emphasized its importance in the overall pathway. Although the conformational closing of pol β before chemistry appears unaffected by the 8-oxo group compared to that in the **G**:**C** system (22), the active-site geometry in the former 8-oxo**G** system deviates further from the reaction-competent state than does the latter complex. Therefore, the energy barriers associated with the pre-chemistry avenue may be larger for the lesioned complex; this difference in energy might contribute to the lower efficiency of d**C**TP incorporation opposite 8-oxo**G** than opposite d**G** in pol β (12) (efficiency ratio of 1:4).

In addition, we find that Tyr[271] competes for the incoming nucleotide site when d**A**TP pairs with a *syn* 8-oxo**G**; the unfavorable interactions result in large distortions in the active site destabilizing the closed state. Hence, Tyr[271] might cause the slow thumb closing and lower insertion efficiency of d**A**TP than d**C**TP opposite 8-oxo**G**. A site-directed mutagenesis experiment on Tyr[271] (e.g., Tyr[271]Ala) might help verify the function of Tyr[271] in pol β's selection of d**C**TP against d**A**TP. In fact, a recent mutagenesis experiment has found that mutating Lys[536] of T7 DNA polymerase to alanine switches the d**C**TP/d**A**TP preference (15); Lys[536] is a recognized residue that interacts with the templating base.

Structural and kinetic data for correct and incorrect d**N**TP incorporation in various DNA polymerases show that details of the overall reaction profile of these enzymes and the rate-limiting step are case-dependent (see (52) and therein). For pol β, in particular, experimental measurements using fluorescence-based techniques could not determine exclusively which step is rate-limiting (53,54). Prior dynamics simulations (22–24,27,28,51) suggest that the conformational changes before the chemical reaction are rapid and not likely rate-limiting. Our QM/MM studies of the correct (d**C**TP) and incorrect (d**A**TP) incorporations opposite **G** (51,55) indicate that the chemical step is rate-limiting for both cases. Particularly, pol β's fidelity discrimination is achieved by destabilizing the closed state and increasing the free energy barrier for the deprotonation of 3′-OH when d**A**TP is incorporated opposite **G**. Since the thumb closing/opening motions in the 8-oxo**G** pol β complexes occur over nanosecond range, the subtle rearrangements for the divalent metal ions as well as the following nucleotidyl-transfer reaction might be rate-limiting in these complexes. Yet all conformational

steps and subtle residue motions that lead to the closed conformation of pol β can affect the reaction efficiency and fidelity.

The partially open form of pol β in the simulated 8-oxo**G** (*syn*):d**A**TP system suggests higher free energy barriers for thumb closing. This might increase the dissociation rate of d**A**TP from the active site and lower the binding affinity and incorporation efficiency of d**A**TP opposite 8-oxo**G**. Further, our simulations also reveal that pol β achieves a more closed conformation when a *syn* rather than *anti* 8-oxo**G** unit pairs with d**A**TP. Because a **G**:d**A**TP mismatch would resemble the 8-oxo**G** (*anti*):d**A**TP pair, a more solvent-exposed active site in a **G**:d**A**TP system would explain the low insertion efficiencies of d**A**TP opposite **G** compared to 8-oxo**G** (12).

Taken together, our series of dynamics simulations comparing incorporation of d**A**TP versus d**C**TP opposite 8-oxo**G** as well as d**C**TP opposite the lesioned versus nonlesioned template guanine suggest how pol β's closing and opening conformational pathways affect its fidelity mechanism when processing 8-oxo**G**. A separate transition path sampling work (29) provides further insights regarding the preference ratio (2:1 from (12)). The delineated pathways of the thumb closing for the two 8-oxo**G** complexes suggest that distinct sequences and energy barriers associated with the conformational events in the 8-oxo**G** complexes lead to closed forms with different stability and thus different insertion efficiencies (29).

Of course, the MD simulations are never long enough in relation to pol β's function in vivo, so the captured thumb motions only suggest trends (i.e., the preference of the open and closed states of thumb). Force-field imperfections and modeling approximations also apply to all dynamics simulations. Nevertheless, our trajectories clearly distinguish conformational profiles when pol β inserts different incoming nucleotides (d**A**TP or d**C**TP) opposite the 8-oxo**G**, and also help interpret existing crystal structures of pol β (13,17) with mismatches. The general question of whether mismatched systems actually attain closed state or whether the chemical reaction can proceed from a partially open or open state is an important challenge for future investigations. This question likely corresponds to our notion of the pre-chemistry avenue (51) in which high barriers that are basepair- and system-dependent must be overcome to reach the chemical-reaction competent state.

SUPPLEMENTARY MATERIAL

An online supplement to this article can be found by visiting BJ Online at http://www.biophysj.org. This material consists of RMSD plots of pol β's α-helix N in all simulations before and after the chemical reaction; time evolution of backbone dihedral angles of Phe[272] and Arg[258] in all simulations before and after the chemical reaction; and the proposed ideal ''two-metal-ion catalysis'' geometry.

REFERENCES

1. Mol, C. D., S. S. Parikh, C. D. Putnam, T. P. Lo, and J. A. Tainer. 1999. DNA repair mechanisms for the recognition and removal of damaged DNA bases. *Annu. Rev. Biophys. Biomol. Struct.* 28:101–128.

2. Lindahl, T. 1993. Instability and decay of the primary structure of DNA. *Nature.* 362:709–715.

3. Harman, D. 1981. The aging process. *Proc. Natl. Acad. Sci. USA.* 78:7124–7128.

4. Ames, B. N. 1983. Dietary carcinogens and anticarcinogens—oxygen radicals and degenerative diseases. *Science.* 221:1256–1264.

5. Greenblatt, M. S., W. P. Bennett, M. Hollstein, and C. C. Harris. 1994. Mutations in the p53 tumor suppressor gene: clues to cancer etiology and molecular pathogenesis. *Cancer Res.* 54:4855–4878.

6. Hainaut, P. 1998. Database of p53 gene mutations in human tumors and cell lines: updated compilation, revised formats and new visualization tools. *Nucleic Acids Res.* 26:205–213.

7. Shibutani, S., M. Takeshita, and A. P. Grollman. 1991. Insertion of specific bases during DNA synthesis past the oxidation-damaged base 8-oxodG. *Nature.* 349:431–434.

8. Lowe, L. G., and F. P. Guengerich. 1996. Steady-state and pre-steady state kinetic analysis of dNTP insertion opposite 8-oxo-7,8-dihydroguanine by *Escherichia coli* polymerase I exo- and II exo. *Biochemistry.* 35:9840–9849.

9. Furge, L. L., and F. P. Guengerich. 1997. Analysis of nucleotide insertion and extension at 8-oxo-7,8-dihydroguanine by replicative T7 polymerase exo- and human immunodeficiency virus-1 reverse transcriptase using steady-state and pre-steady-state kinetics. *Biochemistry.* 21:6475–6487.

10. Freisinger, E., A. P. Grollman, H. Miller, and C. Kisker. 2004. Lesion (in)tolerance reveals insights into DNA replication fidelity. *EMBO J.* 23:1494–1505.

11. Hsu, G. W., M. Ober, T. Carell, and L. S. Beese. 2004. Error-prone replication of oxidatively damaged DNA by a high-fidelity DNA polymerase. *Nature.* 431:217–221.

12. Miller, H., R. Prasad, S. H. Wilson, F. Johnson, and A. P. Grollman. 2000. 8-oxodGTP incorporation by DNA polymerase β is modified by active-site residue Asn^{279}. *Biochemistry.* 39:1029–1033.

13. Krahn, J. M., W. A. Beard, H. Miller, A. P. Grollman, and S. H. Wilson. 2003. Structure of DNA polymerase β with the mutagenic DNA lesion 8-oxodeoxyguanine reveals structural insights into its coding potential. *Structure.* 11:121–127.

14. Brieba, L. G., B. F. Eichman, R. J. Kokoska, S. Doublie, T. A. Kunkel, and T. Ellenberger. 2004. Structural basis for the dual coding of potential of 8-oxoguanosine by a high-fidelity DNA polymerase. *EMBO J.* 23:3452–3461.

15. Brieba, L. G., R. J. Kokoska, K. Bebenek, T. A. Kunkel, and T. Ellenberger. 2005. A lysine residue in the fingers subdomain of T7 DNA polymerase modulates the miscoding potential of 8-oxo-7, 8-dihydroguanosine. *Structure.* 13:1653–1659.

16. Rechkoblit, O., L. Malinina, Y. Cheng, V. Kuryavyi, S. Broyde, N. Geacintov, and D. J. Patel. 2006. Stepwise translocation of Dpo4 polymerase during error-free bypass of an oxoG lesion. *PLoS Biol.* 4:25–42.

17. Krahn, J. M., W. A. Beard, and S. H. Wilson. 2004. Structural insights into DNA polymerase deterrents for misincorporation support an induced-fit mechanism for fidelity. *Structure.* 12:1823–1832.

18. Doublié, S., and T. Ellenberger. 1998. The mechanism of action of T7 DNA polymerase. *Curr. Opin. Struct. Biol.* 8:704–712.

19. Sawaya, M. R., R. Prasad, S. H. Wilson, J. Kraut, and H. Pelletier. 1997. Crystal structures of human DNA polymerase β complexed with gapped and nicked DNA: evidence for an induced fit mechanism. *Biochemistry.* 36:11205–11215.

20. Li, Y., S. Korolev, and G. Waksman. 1998. Crystal structures of open and closed forms of binary and ternary complexes of the large fragment of *Thermus aquaticus* DNA polymerase I: structural basis for nucleotide incorporation. *EMBO J.* 17:7514–7525.

21. Beard, W. A., and S. H. Wilson. 1998. Structural insights into DNA polymerase β fidelity: hold tight if you want it right. *Chem. Biol.* 5:R7–R13.

22. Arora, K., and T. Schlick. 2004. *In silico* evidence for DNA polymerase β's substrate-induced conformational change. *Biophys. J.* 87:1–13.

23. Yang, L., W. A. Beard, S. H. Wilson, S. Broyde, and T. Schlick. 2002. Polymerase β simulations suggest that Arg^{258} rotation is a slow step rather than large subdomain motion *per se*. *J. Mol. Biol.* 317:651–671.

24. Yang, L., W. A. Beard, S. H. Wilson, B. Roux, S. Broyde, and T. Schlick. 2002. Local deformations revealed by dynamics simulations of DNA polymerase β with DNA mismatches at the primer terminus. *J. Mol. Biol.* 321:459–478.

25. Yang, L., W. A. Beard, S. H. Wilson, S. Broyde, and T. Schlick. 2004. The highly organized but pliant active-site of DNA polymerase β: compensatory interaction mechanisms in mutant enzymes by dynamics simulations and energy analysis. *Biophys. J.* 86:3392–3408.

26. Yang, L., K. Arora, W. A. Beard, S. H. Wilson, and T. Schlick. 2004. The critical role of magnesium ions in DNA polymerase β's closing and active site assembly. *J. Am. Chem. Soc.* 126:8441–8453.

27. Radhakrishnan, R., and T. Schlick. 2004. Orchestration of cooperative events in DNA synthesis and repair mechanism unraveled by transition path sampling of DNA polymerase β's closing. *Proc. Natl. Acad. Sci. USA.* 101:5970–5975.

28. Radhakrishnan, R., and T. Schlick. 2005. Fidelity discrimination in DNA polymerase β: differing closing profiles for a mismatched G:A versus matched G:C basepair. *J. Am. Chem. Soc.* 127:13245–13252.

29. Wang, Y., and T. Schlick. 2007. Distinct energetics and closing pathways for DNA polymerase β with 8-oxo**G** template and different incoming nucleotides. *BMC Struct. Biol.*

30. Kouchakdjian, M., V. Bodepudi, S. Shibutani, M. Eisenberg, F. Johnson, A. P. Grollman, and J. J. Patel. 1991. NMR structural studies of the ionizing radiation adduct 7-hydro-8-oxodeoxyguanosine (8-oxog-7H-dG) opposite deoxyadenosine in a DNA duplex. 8-Oxo-7H-dG(*syn*)·dA(*anti*) alignment at lesion site. *Biochemistry.* 30:1403–1412.

31. Brünger, A. T., and M. Karplus. 1988. Polar hydrogen positions in proteins: empirical energy placement and neutron diffraction comparison. *Proteins Struct. Funct. Genet.* 4:148–156.

32. Brooks, B. R., R. E. Bruccoleri, B. D. Olafson, D. J. States, S. Swaminathan, and M. Karplus. 1983. CHARMM: a program for macromolecular energy, minimization, and dynamics calculations. *J. Comput. Chem.* 4:187–217.

33. MacKerell, A. D., Jr., and N. K. Banavali. 2000. All-atom empirical force field for nucleic acids. II. Application to molecular dynamics simulations of DNA and RNA in solution. *J. Comput. Chem.* 21: 105–120.

34. Mezei, M. 1997. Optimal position of solute for simulations. *J. Comput. Chem.* 18:812–815.

35. Qian, X., D. Strahs, and T. Schlick. 2001. A new program for optimizing periodic boundary models of solvated biomolecules (PBCAID). *J. Comput. Chem.* 22:1843–1850.

36. Klapper, I., R. Hagstrom, R. Fine, K. Sharp, and B. Honig. 1986. Focusing of electric fields in the active site of Cu-Zn superoxide dismutase: effects of ion strength and amino-acid modification. *Proteins.* 1:47–59.

37. Gilson, M. K., K. Sharp, and B. H. Honig. 1988. Calculating the electrostatic potential of molecules in solution: method and error assessment. *J. Comput. Chem.* 9:327–335.

38. Wang, Y., K. Arora, and T. Schlick. 2006. Subtle but variable conformational rearrangements in the replication cycle of *Sulfolobus solfataricus* P2 DNA polymerase IV (Dpo4) may accommodate lesion bypass. *Protein Sci.* 15:135–151.

39. Norberg, J., and L. Nilsson. 2000. On the truncation of long-range electrostatic interactions in DNA. *Biophys. J.* 79:1537–1553.

40. Schlick, T., E. Barth, and M. Mandziuk. 1997. Biomolecular dynamics at long timesteps: bridging the timescale gap between simulation and experimentation. *Annu. Rev. Biophys. Biomol. Struct.* 26:181–222.

41. Barth, E., and T. Schlick. 1998. Overcoming stability limitation in biomolecular dynamics. I. Combining force splitting via extrapolation with Langevin dynamics in LN. *J. Chem. Phys.* 109:1617–1632.

42. Barth, E., and T. Schlick. 1998. Extrapolation versus impulse in multiple-timestepping schemes. II. Linear analysis and applications to Newtonian and Langevin dynamics. *J. Chem. Phys.* 109:1633–1642.

43. Schlick, T. 2001. Time-trimming tricks for dynamic simulations: splitting force updates to reduce computational work. *Structure.* 9: R45–R53.

44. Steitz, T. A. 1999. DNA polymerases: structural diversity and common mechanisms. *J. Biol. Chem.* 274:17395–17398.

45. Batra, V. K., W. A. Beard, D. D. Shock, J. M. Krahn, L. C. Pedersen, and S. H. Wilson. 2006. Magnesium induced assembly of a complete DNA polymerase catalytic complex. *Structure.* 14:757–766.

46. Mildvan, A. S. 1997. Mechanisms of signaling and related enzymes. *Proteins Struct. Funct. Genet.* 29:401–416.

47. Batra, V., W. A. Beard, D. D. Shock, L. C. Pederson, and S. H. Wilson. 2005. Nucleotide-induced DNA polymerase active site motions accommodating a mutagenic DNA intermediate. *Structure.* 13:1225–1233.

48. Arora, K., W. A. Beard, S. H. Wilson, and T. Schlick. 2005. Mismatch-induced conformational changes in polymerase β/DNA complex support an induced-fit mechanism for fidelity. *Biochemistry.* 44:13328–13341.

49. Vaisman, A., H. Ling, R. Woodgate, and W. Yang. 2005. Fidelity of Dpo4: effect of metal ions, nucleotide selection and pyrophosphorolysis. *EMBO J.* 24:2957–2967.

50. Rothwell, P. J., V. Mitaksov, and G. Waksman. 2005. Motions of the fingers subdomain of Klentaq1 are fast and not rate limiting: implications for the molecular basis of fidelity in DNA polymerases. *Mol. Cell.* 19:345–355.

51. Radhakrishnan, R., K. Arora, Y. Wang, W. A. Beard, S. H. Wilson, and T. Schlick. 2006. Regulation of DNA repair fidelity by molecular checkpoints: ''gates'' in DNA polymerase β's substrate selection. *Biochemistry.* 45:15142–15156.

52. Joyce, C. M., and S. J. Benkovic. 2004. DNA polymerase fidelity: kinetics, structure, and checkpoints. *Biochemistry.* 43:14317–14324.

53. Arndt, J. W., W. Gong, X. Zhong, A. K. Showalter, J. Liu, C. A. Dunlap, Z. Lin, C. Paxson, M.-D. Tsai, and M. K. Chan. 2001. Insight into the catalytic mechanism of DNA polymerase β: structures of intermediate complexes. *Biochemistry.* 40:5368–5375.

54. Dunlap, C. A., and M. D. Tsai. 2002. Use of 2-aminopurine and tryptophan fluorescence as probes in kinetic analyses of DNA polymerase β. *Biochemistry.* 41:11226–11235.

55. Radhakrishnan, R., and T. Schlick. 2006. Correct and incorrect nucleotide incorporation pathways in DNA polymerase β. *Biochem. Biophys. Res. Commun.* 350:521–529.

56. Humphrey, W., A. Dalke, and K. Schulten. 1996. VMD—visual molecular dynamics. *J. Mol. Graph.* 14:33–38.